Tellus (2000), 52A, 162–180
Printed in UK. All rights reserved

TELLUS
ISSN 0280–6495

Numerical simulations of the Piedmont flood of 4–6 November 1994

By ROSSELLA FERRETTI[1], *Department of Physics, University of L'Aquila, Via Vetoio, 67010 Coppito-L'Aquila, Italy;* SIMON LOW-NAM and RICHARD ROTUNNO, *National Center for Atmospheric Research*, Boulder, CO 80307, USA*

(Manuscript received 16 December 1998; in final form 20 July 1999)

ABSTRACT

A case study of the 1994 Piedmont flood is carried out by performing several numerical experiments using the MM5 model. We report on sensitivity tests and analyses that suggest the following description of the events leading to the flood: rising motion ahead of an upper-level trough, progressing from Spain towards Italy, initiated deep convection within the conditionally unstable air existing over the Mediterranean. Thus, a band of intense precipitation and low-level southerly winds formed and moved eastward with the upper trough. As the rain band and strong southerlies encountered the western Alps, moist air was lifted, resulting in large amounts of rainfall. The associated latent-heat-related upward motion produced a strong positive vorticity anomaly over the western Alps with associated low-level easterlies in the Po Valley which appear to have played a major role in retarding the generally eastward progress of the rain band over Piedmont.

1. Introduction

A major goal of the Mesoscale Alpine Programme (MAP; see Binder et al. (1996)) is to secure an improved ability to predict severe flooding in the Alpine region. Therefore, a central research focus of MAP is the understanding of the contributing meteorological factors. In preparation for the MAP field campaign, the meteorological conditions of four recent flooding events (22 September 1992, Vaison-La-Romaine, France; 24 September 1993, Brig, and 13–14 September, South Ticino, Switzerland; 5–6 November 1994, Piedmont, Italy) have been the subjects of several recent studies. Massacand et al. (1998) showed that in all four cases the synoptic-scale flow was characterized by a meridionally elongated, upper-level potential-vorticity anomaly (or pressure trough) which moved slowly from west to east. In an analysis of the Vaison-La-Romaine case, Senesi et al. (1996) found that the heavy rain was generated by several mesoscale convective systems located ahead of the surface cold front associated with the upper-level pressure trough; timing and location of the convective systems appeared to be strongly influenced by local orography. Meteorological analysis of the Piedmont case by Doswell et al. (1998), and simulations by Buzzi et al. (1998) and Romero et al. (1998), indicate that the flooding rains are mainly orographically generated with convection playing an important role only in the coastal zone.

The purpose of this paper is to use numerical-simulation experiments of the Piedmont flood to contribute to the general MAP objective of achieving a better understanding of the meteorological factors involved in severe flooding of the Alpine

[1] Corresponding author.
e-mail: rossella.ferretti@aquila.infn.it
* The National Center for Atmospheric Research is sponsored by the National Science Foundation.

region. The apparent importance of both the large-scale dynamics and the embedded cumulus convection motivated us to experiment with the Emanuel (1991, 1993) cumulus scheme (version 2.3, K. Emanuel, personal communication), as it is designed with particular attention to situations where cumulus convection acts in response to synoptic-scale destabilization. The Emanuel cumulus scheme has been successfully used in two different mesoscale models (Buzzi et al., 1998; Romero et al., 1998). The present model simulation of the Piedmont flood also uses the Emanuel scheme (CTRL) which has been newly implemented.

The plan of the present paper is as follows. A brief description of the synoptic and mesoscale features of the Piedmont flood is given in Section 2. The numerical simulations and special sensitivity experiments are described in Section 3. In Section 4, we report the model simulation of the Piedmont flood. The simulations are performed using a coarse mesh (horizontal grid length = 30 km) covering the domain shown in Fig. 1 with an embedded fine mesh (horizontal grid length = 10 km) centered on Piedmont (Fig. 1) where the flooding occurred. Through analysis and sensitivity experiments, we attempt in Section 5 to identify the relative importance of the several factors which seem to have contributed significantly to the flood in the Piedmont area. A summary of the present findings is contained in Section 6.

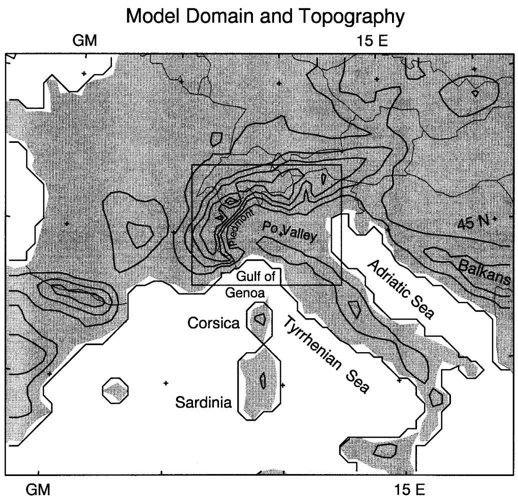

Fig. 1. Model domain and constant-height contours (c.i. = 500 m) of model topography. Horizontal grid resolution over the model domain is 30 km, except within the smaller domain, indicated by the box, in which the horizontal resolution is 10 km.

2. Case description

The European Centre for Medium Range Forecasting (ECMWF) analysis at 0.5° of the synoptic-scale meteorological conditions attending the Piedmont flood are summarized in Fig. 2. The upper-level flow is characterized by a large-amplitude wave in the 500 hPa height field (Fig. 2a) and the 850 hPa temperature field (Fig. 2b) at 1200 UTC 4 November 1994. The warm sector of the temperature wave is located over western Europe, eastward from the upper-level trough axis, which is located over Portugal; there is a cold front (the zone of strong temperature contrast) at the western edge of the Mediterranean. Over the course of the following 36h (Figs. 2c, d), the upper-level-trough axis and the cold front migrate toward Italy while the downstream ridge over eastern Europe, and the cold air over Eurasia, remain relatively stationary. The relatively stationary anticyclone over eastern Europe, together with the eastward-moving trough, imply a contraction of the zonal wavelength of the upper wave. Moreover, the surface-pressure field (Figs. 2b and 2d) indicates that there is an intensification of the relatively stationary high-pressure area (note the stationarity of the 1020 hPa contour over Italy) over the Balkans. Hence the warm tongue in the 850 hPa temperature contracts in the zonal direction over Italy as its eastward movement is resisted by the flow associated with the surface anticyclone.

Downstream of the advancing upper-level wave over the western Mediterranean there is a moist air mass. Fig. 3 contains the ECMWF analysis of the water-vapor mixing ratio q_v and winds at 850 hPa. The southerly winds associated with the upper trough and cold front advect moisture-laden air toward western Europe. In particular, the moist air stream progresses eastward to the location where one might expect a strong orographic enhancement of rainfall as the southerly stream impinges on the western Alps.

Through an analysis of IR satellite imagery and the SSM/I (Special Sensor Microwave/Imager) system, Boni et al. (1996) were able to identify the

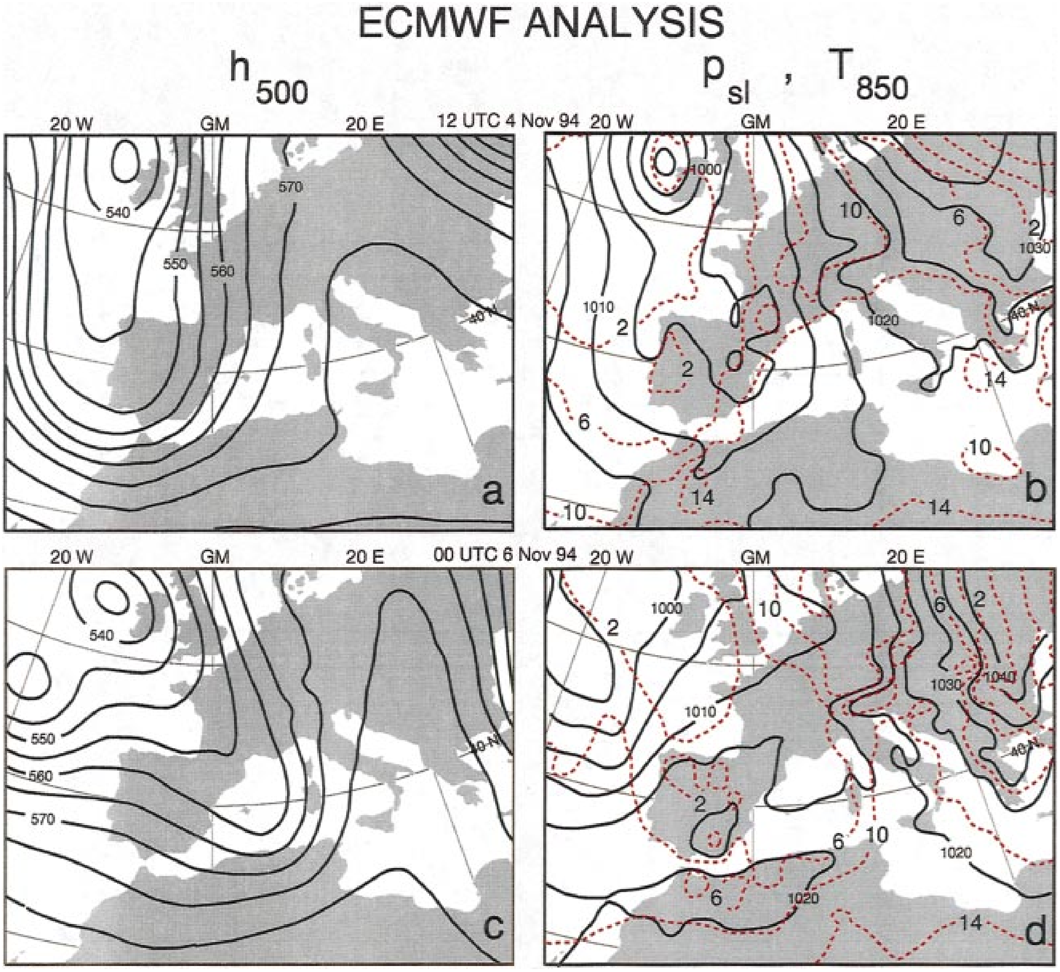

Fig. 2. ECMWF analysis of the 500 hPa-height field h_{500} (c.i. = 50 m, the trailing digit "0" is dropped on the contour label) at (a) 1200 UTC 4 November 1994 and (c) 0000 UTC 6 November 1994, and sea-level pressure field (c.i. = 5 hPa) and 850 hPa-temperature field T_{850} (dashed lines, c.i. = 4 C) at (b) 1200 UTC 4 November 1994 and (d) 0000 UTC 6 November 1994.

areas where convection was embedded in the large-scale cloud field. Their results indicate (see their Fig. 12) that there is convection concentrated within the relatively narrow, north-south oriented, eastward-moving cloud band shown in Fig. 4. The latter band appears to move eastward in step with the upper-level wave. At 1200 UTC, the band reached the west coast of Sardinia, and by 1800 UTC the convection extended along a line south-southeastward from the western Alps, toward the east side of Corsica and Sardinia.

Fig. 5a shows the station precipitation data accumulated over the 24-h period ending 0600 UTC 5 November 1994 obtained from the MAP data archive. Two areas of heavy precipitation are evident, one extends from the central part of France towards the Mediterranean sea, and the other extends from southeastern France into the Piedmont region. These observations indicate that precipitation was occurring over the Piedmont region well ahead of the approaching frontal system. The line of precipitation over France is also suggested by the satellite picture (Fig. 4a) as a band of clouds (cf. Fig. 7 of Boni et al., 1996)

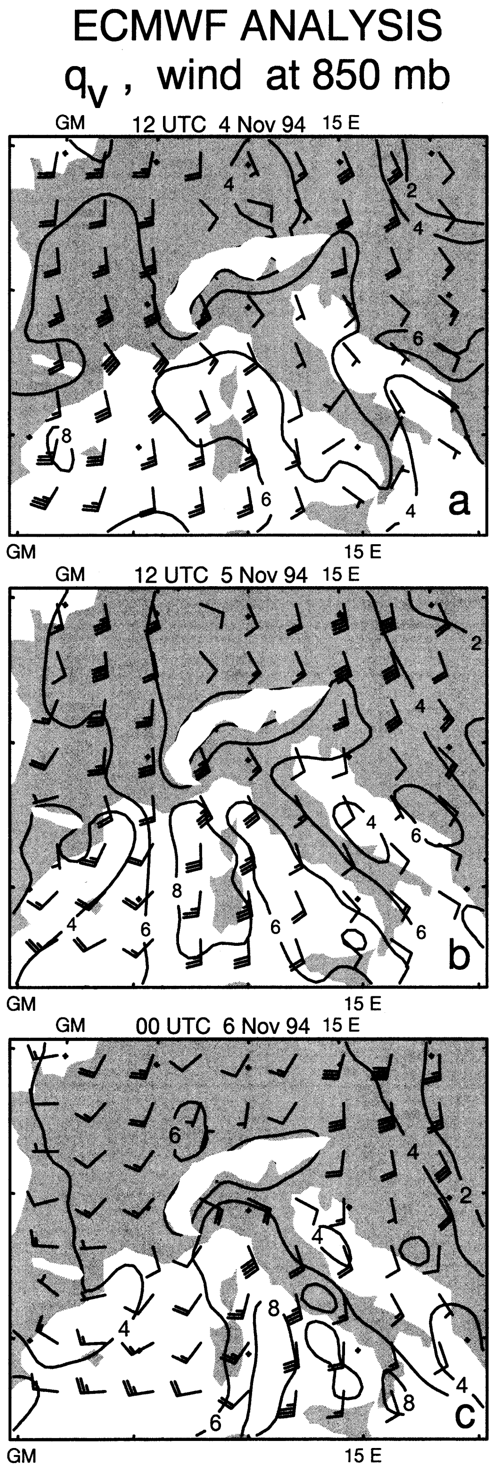

that extends well into the Mediterranean sea. In the next 24-h accumulation ending at 0600 UTC 6 November 1994 (Fig. 5b), the heavy precipitation reached the western slopes of the Alps; three stations (heavy black stars) in the Piedmont region reported a 24-h accumulation well in excess of 300 mm. Fig. 5b also shows that the band of precipitation extended southeastward over the Mediterranean. At this time the northern stations over Corsica were reporting precipitation amounts in excess of 200 mm. The infrared satellite picture valid at 1800 UTC 5 November (Fig. 4c) shows a cloud band extending southward over an area greater than that in evidence six hours earlier (Fig. 4b); Fig. 12 of Boni et al. (1996) indicates that the the aforementoned cloud band is associated with cold cloud tops.

3. Model characteristics and experiment design

The numerical simulations are carried out using the Penn State/NCAR mesoscale model (MM5), which is a nonhydrostatic, primitive-equation model with a terrain-following vertical coordinate (Dudhia, 1993). The model has multiple-nesting capabilities to enhance the simulation over the area of interest.

In this study, the CTRL uses the newly implemented Emanuel (1993) scheme to parameterize the subgrid-scale convection, while the explicit prediction of resolvable microphysics fields of cloud, rain water, and ice are done according to the simple scheme of Dudhia (1989). Other physical parameterizations used in the model include the Blackadar planetary boundary layer (Zhang and Anthes, 1982), surface energy fluxes and atmospheric radiation (Benjamin, 1983).

The computational domain (Fig. 1) has 51×61 grid points in the north-south and east-west direction respectively, with a horizontal grid spacing of 30 km. Within this coarse-mesh domain, a finer 10-km grid is embedded and centered over the

Fig. 3. ECMWF analysis of the water-vapor mixing ratio q_v (c.i. = 2 gm Kg^{-1}) and wind (one barb = 10 knots) at 850 hPa at (a) 1200 UTC 4 November 1994, (b) 1200 UTC 5 November 1994, and (c) 0000 UTC 6 November 1994. Here and in the following, terrain height exceeding the 850 hPa level is indicated by the blank areas.

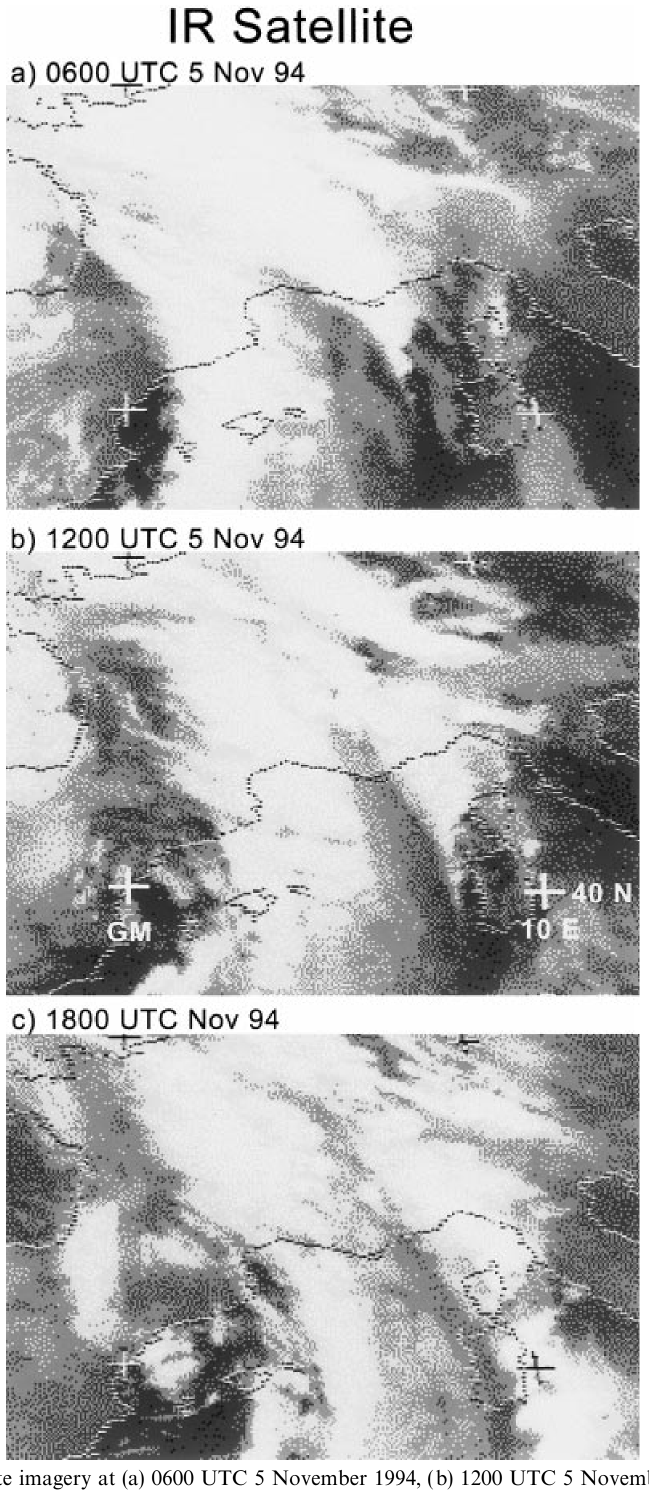

Fig. 4. Infrared satellite imagery at (a) 0600 UTC 5 November 1994, (b) 1200 UTC 5 November 1994, and (c) 1800 UTC 5 November 1994.

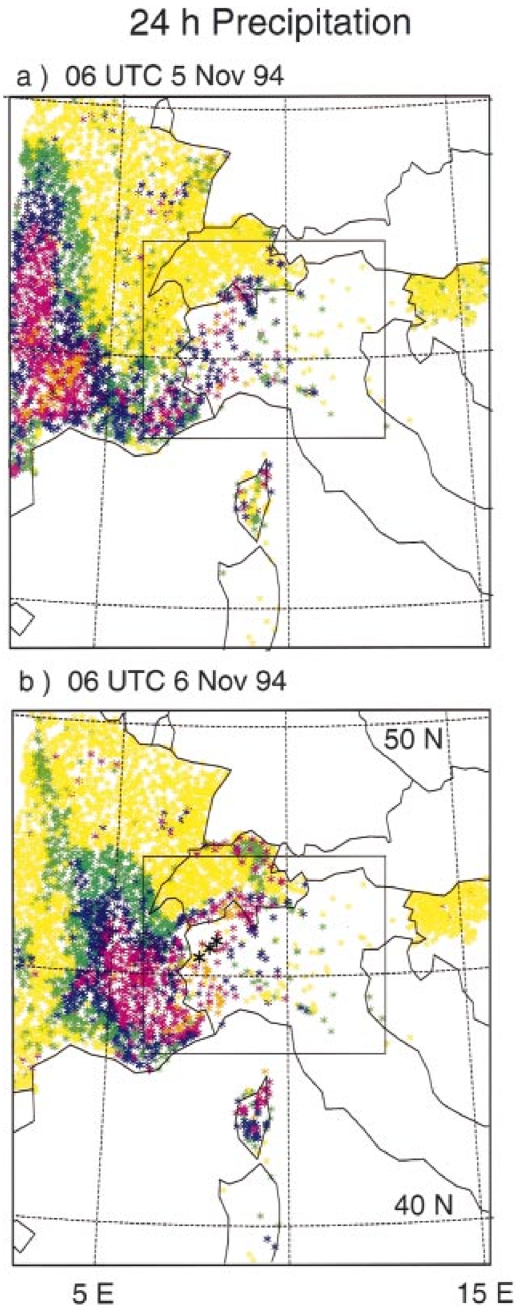

Fig. 5. Observed accumulated precipitation (mm) over the 24-h period ending (a) 0600 UTC 5 November 1994 and (b) 0600 UTC 6 November 1994. The code color is : 0–1 mm yellow; 1–25 mm green; 25–50 mm blue; 50–100 mm purple; 100–200 mm orange; >200 mm red; >300 mm black.

Alps to better resolve the complex orographic flow in this region. In the vertical, the model has 23 unevenly spaced layers with more levels being placed in the boundary layer. The lowest model level is about 40 m above the ground.

To examine the relative roles of latent-heat release and topography, we carried out several experiments in an attempt to isolate their relative effects. To assess the effect of latent-heat release, we perform an experiment in which latent-heating is set to zero, while keeping everything else identical to the CTRL; this experiment is referred to as the fake-dry run (FDRY). To test the role of topography to this flood event, we conducted an experiment with the land surface set to a uniform height of 100 m (NALPS). All the simulations use the same initial and boundary conditions, which are derived from the National Centers for Environmental Prediction (NCEP) global data analyses on a 2.5° resolution. The 12-hourly NCEP analyses are interpolated to MM5 lambert conformal grids to provide both the initial condition at 1200 UTC 4 November 1994, and the 12-h lateral boundary conditions to the 30-km domain. The inner 10-km domain obtains its lateral boundary conditions from the 30-km domain during the model integration. All the simulations start at 1200 UTC 4 November 1994 and integrate for a 48 h period ending at 1200 UTC 6 November 1994. In the following section we compare the NCEP-initialized model results with the independent ECMWF analysis discussed in Section 2.

4. Model verification

The model simulated 500 hPa height field (not shown) shows good agreement to the analyses. In particular at upper levels, the rotation of the trough axis, and the maintenance of the ridge over the Balkans, compare well with the ECMWF analyses shown in Fig. 2. The CTRL surface pressure field (not shown) also exhibits very good agreement with the ECMWF analyses to the extent that even the relative stationarity of the 1020 hPa contour line over Italy is simulated.

Overall agreement between the model-predicted q_v (Fig. 6) and the ECMWF analyzed fields (Fig. 3) is good with both showing the intense zonal contraction with time of the moist sector accompanied by enhanced southerly winds. Note the placement of the moist sector just south of the western Alps, and the tendency for the northern part of the moist sector to lag behind the generally eastward progress of the southern part.

Most of the model precipitation occurred in association with a relatively narrow band of rising motion. To show that there is a general correspondence between the model-produced band and that which occurred on 5 November 1994, we show the integrated cloud water field in Fig. 7 at times that are coincident with the infrared satellite images shown in Fig. 4. At 0600 UTC, Fig. 7a shows there is an intense line of integrated cloud water in CTRL that roughly corresponds to the narrow cloud line in evidence in the infrared satellite image shown in Fig. 4a. The small area of cloudiness over southern Europe is missed by the model simulation, however this appears to have no significant consequences for the flooding forecast. The line of integrated cloud water progresses eastward and weakens by 1200 UTC (Fig. 7b), and subsequently at 1800 UTC (Fig. 7c), a narrow line of integrated cloud water forms over Corsica and Sardinia; this evolution is more or less consistent with that shown by the satellite imagery (Figs. 4b, c). Further evidence for the eastward progression of a north-south oriented line and its southward extension towards Corsica and Sardinia is contained in the precipitation data shown in Fig. 5.

The distribution and amount of precipitation is the most difficult quantity of the simulation to verify. Hence most of the discussion here will center on the verification of the model-produced precipitation and the performance of the CTRL.

To compare the model-predicted precipitation with the large-network data shown in Fig. 5, we show in Fig. 8a the CTRL 24 h accumulated precipitation ending at 0600 UTC 6 November 1994 over the entire domain of the simulation (using information only from the coarse grid to depict the larger-scale organization surrounding the flood region, which region will be examined subsequently). Points of similarity with the data shown in Fig. 5 include: precipitation maxima along the southern and western Alps, a line of relatively high precipitation running northwest-

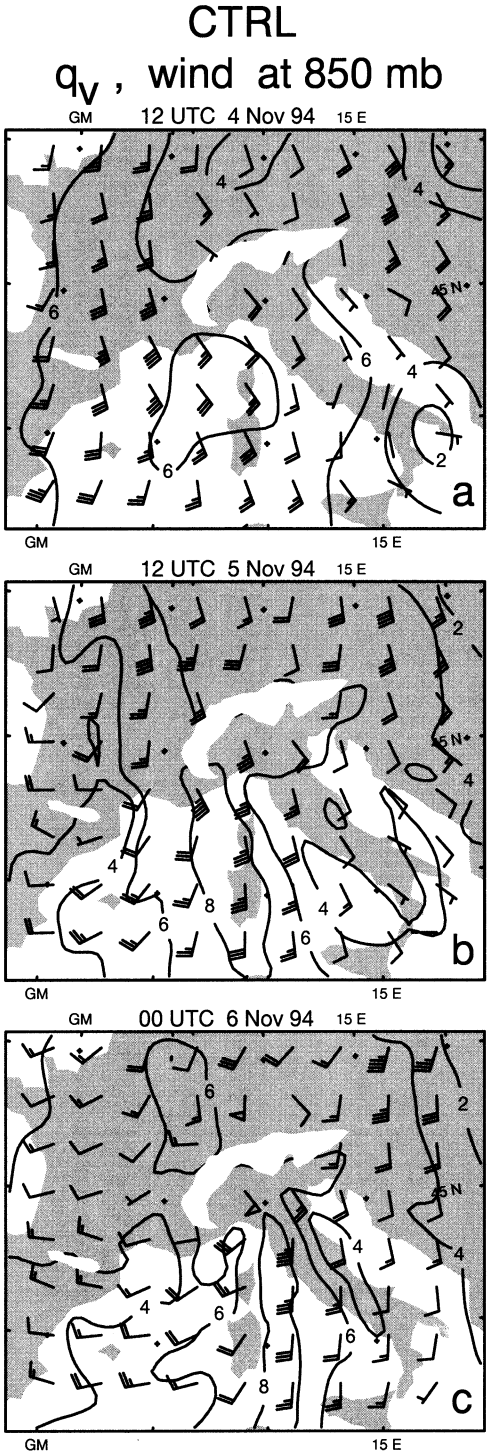

Fig. 6. As in Fig. 3, except for the control simulation in the full model domain.

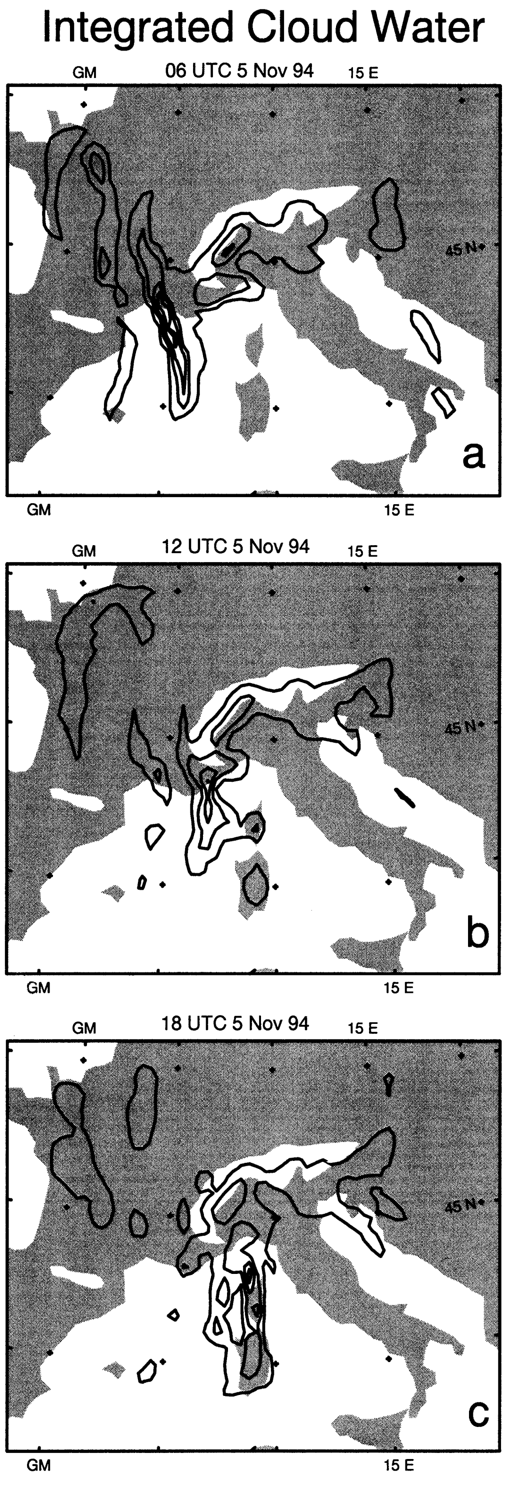

ward through France, and large values of precipitation over Corsica. Of interest is the relatively large amounts of precipitation predicted south of France over the Mediterranean (near 6°E), where unfortunately there is no rain-gauge data. The infrared satellite imagery (Fig. 4a) does suggest, however, that convection was more intense in this region at 0600 UTC, weakened at 1200 UTC as the system moved eastward, and then re-intensified over Corsica at 1800 UTC. Comparing the CTRL total (Fig. 8a) with the CRTL parameterized precipitation (Fig. 8b) shows that the model-predicted heavy-precipitation (>50 mm) features over the Mediterranean are produced by explicitly resolved processes (see below). Analysis of the CTRL parameterized precipitation indicates that the maximum west of Sardinia (Fig. 8b) is due to convection in the post-frontal air mass which, being cooler and drier, is warmed and moistened through sea-surface fluxes. The isolated parameterized precipitation maximum in southeastern Switzerland (Fig. 8b) is due to a convective event that occurred in the model between 1800 UTC 5 November and 0000 UTC 6 November. Interestingly, Fig. 5b shows a local precipitation maximum in this same location.

Fig. 8c displays the 24-h accumulated precipitation for the same period as Fig. 8a, but for the finer 10-km domain. The rainfall amounts and location verify reasonably well against the observations. Fig. 8d shows that the simulations produced precipitation amounts in excess of 300 mm over the 24-h period ending six hours early (0000 UTC 6 November), at nearly the places where such amounts occurred (Fig. 5b). The fine grid (10 km grid spacing) was essential to produce the correct amount and distribution of precipitation; as suggested in Figs. 8a, c, where the fine-grid information is averaged to the coarse grid, the maxima only reach approximately 230 mm. Similar to the findings of Buzzi et al. (1998), where a 30-km grid was used, the location of the precipitation maxima along the coastal mountains, was on the south side rather than the north side, as seen in the observations.

Fig. 7. Vertically integrated cloud water (c.i. = 0.4 mm, first contour line = 0.2 mm) at (a) 0600 UTC 5 November 1994, (b) 1200 UTC 5 November 1994, and (c) 1800 UTC 5 November 1994.

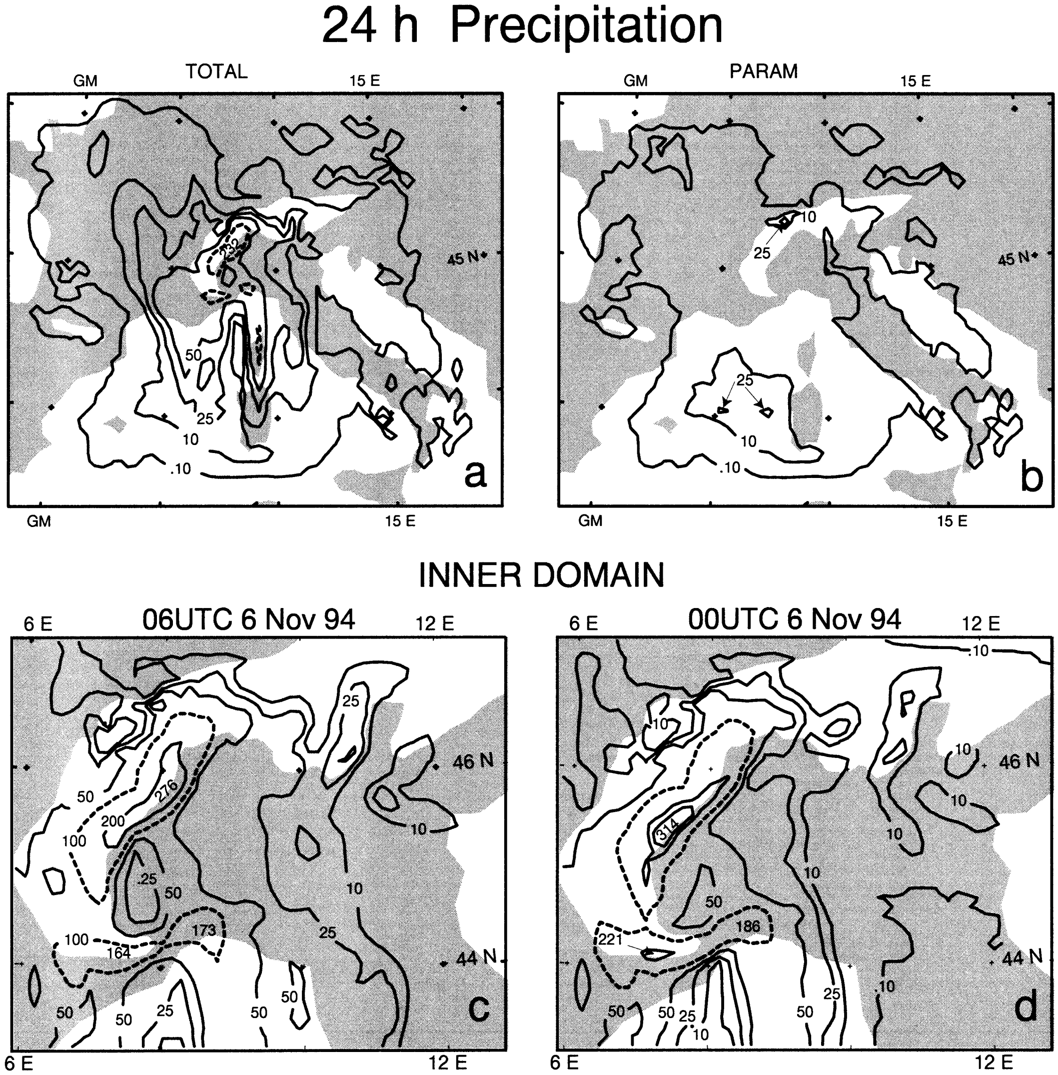

Fig. 8. Accumulated precipitation (mm) over the 24-h period ending on 0600 UTC 6 November 1994 for (a) CTRL total, (b) CTRL parameterization in the coarse domain, (c) CTRL total in the nested domain, and (d) 24-h CTRL total in the nested domain ending on 0000 UTC 6 November 1994.

The fact that the 24-h accumulated precipitation from the CTRL is mainly from the resolved scale, does not necessarily implied that convection was unimportant; it indicates only that the convective motion (thermally direct circulation driven by latent heating) was being computed mainly by the resolved scale in CTRL. As we will show below, the convective instability in the southerly airflow approaching the Alps is mostly removed (by resolved-scaled motions) over the Mediterranean, and hence the flood-producing precipitation over Piedmont is largely due to stable orographic ascent, as noted by Doswell et al. (1998).

Resolved convective motion with a 30-km grid is unrealistic and should be considered a shortcoming of CTRL. However, since the timing and location of the convective motion is strongly regulated by the approaching front, negative consequences of the unrealistic 30km-grid-resolved convection were mininal. In fact, we find it

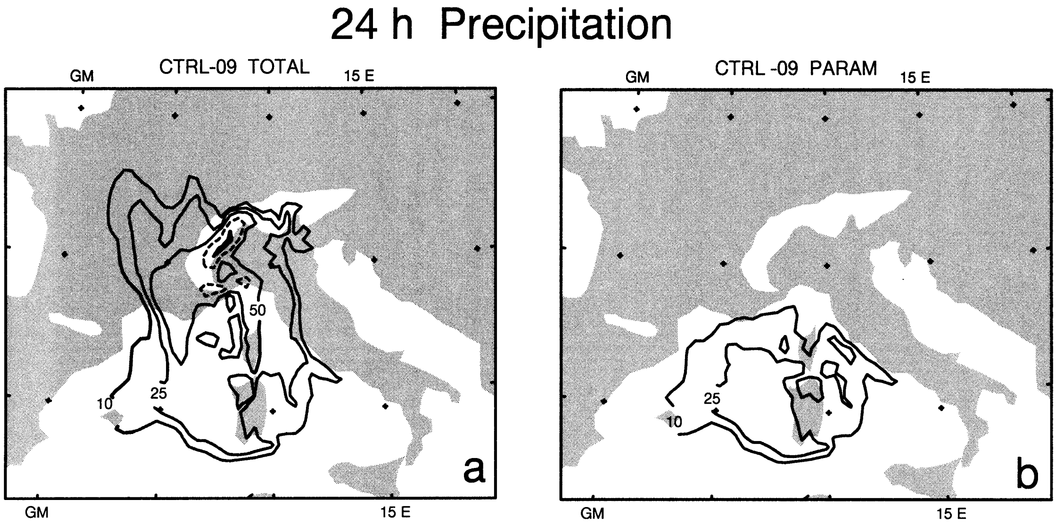

Fig. 9. Accumulated precipitation (mm) over the 24-h period ending on 0600 UTC 6 November 1994 from the (a) CTRL-09 total, and (b) CTRL-09 parameterization.

interesting that the precipitation forecast (mainly from the explicit side) for Corsica using the Emanuel scheme shows a close correspondence to the observations. Although this agreement might be accidental, it might also be that information contained in the large scale was an important contributor to the precise timing and location of the precipitation over the Mediterranean.

To explore this idea a little further we consider that, in the Emanuel scheme, the convective mass flux is driven toward that of the large scale. We believe that in the present case the Emanuel scheme tries to drive the convective mass flux to the relatively small synoptic-scale value, and hence the scheme, although activated, produces weak precipitation. To allow the convective mass flux to behave more independently of the large scale in the Emanuel scheme, we performed an experiment in which the parameter α [see Eq. (16.4.12) of Emanuel 1994] was increased from its present setting of 0.03 (for climate studies) to 0.09 (experiment designated CTRL-09). Fig. 9a shows that the 24-h total rainfall ending 0600 UTC 6 November, over the continent is relatively unaffected; however, the rainfall amount over Corsica is diminished. The convective rainfall in the regions west and east of Corsica in CTRL-09 (Fig. 9b) are much greater than those in CTRL (Fig. 8b). These experiments illustrate that even when there is a strong feature such as front, the distribution of the predicted rain can be sensitive (in this case, over the Mediterranean) to the partitioning of precipitation between explicit and parameterized processes.

5. Analysis and sensitivity experiments

The model version of the meteorological conditions attending the Piedmont flood is summarized in Figs. 10, 11. At 0600 UTC 5 November 1994, Fig. 10a shows a north-south-oriented front over France, and southerly flow over the Mediterranean; an Alps-associated anticyclonic perturbation to the southerly winds is also in evidence. Fig. 11a shows that at this time there is large area of conditionally unstable air* over the Mediterranean. By 0600 UTC, Fig. 11a shows that the rising motion on the forward edge of the advancing upper-level wave (Fig. 2) becomes intense and takes the form of a north-northwest-south-southeast oriented line. At the same time, there is an associated enhancement of the 850 hPa

* The lifted index (LI) is computed as the temperature excess at 500 hPa of the environment with respect to an air parcel lifted moist-adiabatically above the lifted condensation level (LCL).

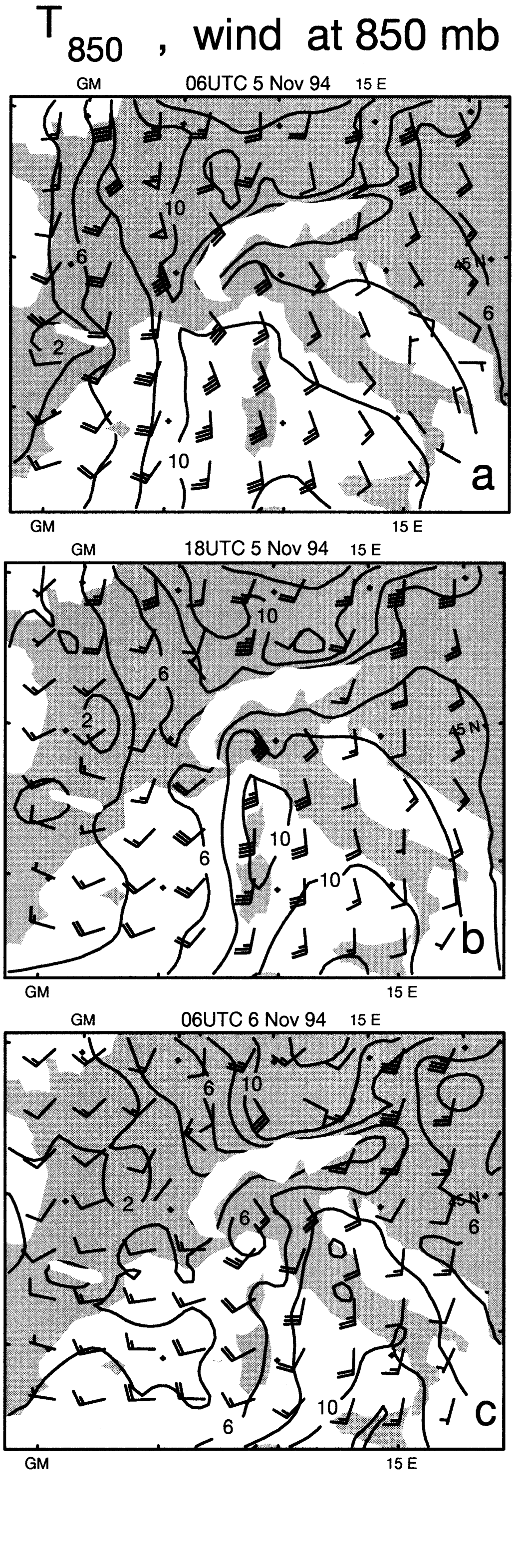

pre-frontal southerly wind (cf. Fig. 10a with Fig. 6a). At 1800 UTC 5 November (Figs. 11b), the region of large conditional instability narrows as it continues its eastward track. Note that although the most unstable air is over the Mediterranean, there is still strong upward motion over the Alps. The relatively long time over which upward motion occurs over the western Alps is associated with the strong easterly wind perturbation over the Po Valley that developed around 1800 UTC 5 November (Fig. 10b). By 0600 UTC 6 November 1994 (Fig. 10c), the front has moved toward north-central Italy, and rainfall over Piedmont has ended; note again the small-scale cyclonic wind perturbation that has formed at the Italian coast near the Gulf of Genoa.

The foregoing description suggests the central importance of latent heating and topographic effects in the explanation of the flooding events. Fig. 12 shows the NALPS and FDRY version of the fields described for the CTRL simulation at 1800 UTC 5 November 1994 (Figs. 10b, 11b). In NALPS, the line of intense rising motion is remarkably close to the position it assumes in CTRL, suggesting the overall synoptic-scale control of the precipitation system. The anticyclonic wind perturbation associated with the Alps is notably absent as the southerly flow is uninterrupted, and carries unstable air over Europe. The rising motion over the location of where the Alps would be, however, is much weaker in NALPS than in CTRL, and only modest amounts of precipitation accumulate there (Fig. 12e). Hence, lifting of air over the Alps must be a critical ingredient in any flood scenario. But before discussing topographic effects, it is convenient to continue now the discussion of those effects of latent heating that are independent of topographic flow.

The NALPS case shown in Fig. 12 suggests that the north-south orientation of the line of precipitation-associated rising motion does not depend on any topographic effect. We believe that this tendency for the narrowing of the region of upward motion is a consequence of the mechanism

Fig. 10. Maps of the control-simulations of the temperature (c.i. = 2 C) and wind (one barb = 10 knots) at 850 hPa at (a) 0600 UTC 5 November 1994, (b) 1800 UTC 5 November 1994, and (c) 0600 UTC 6 November 1994.

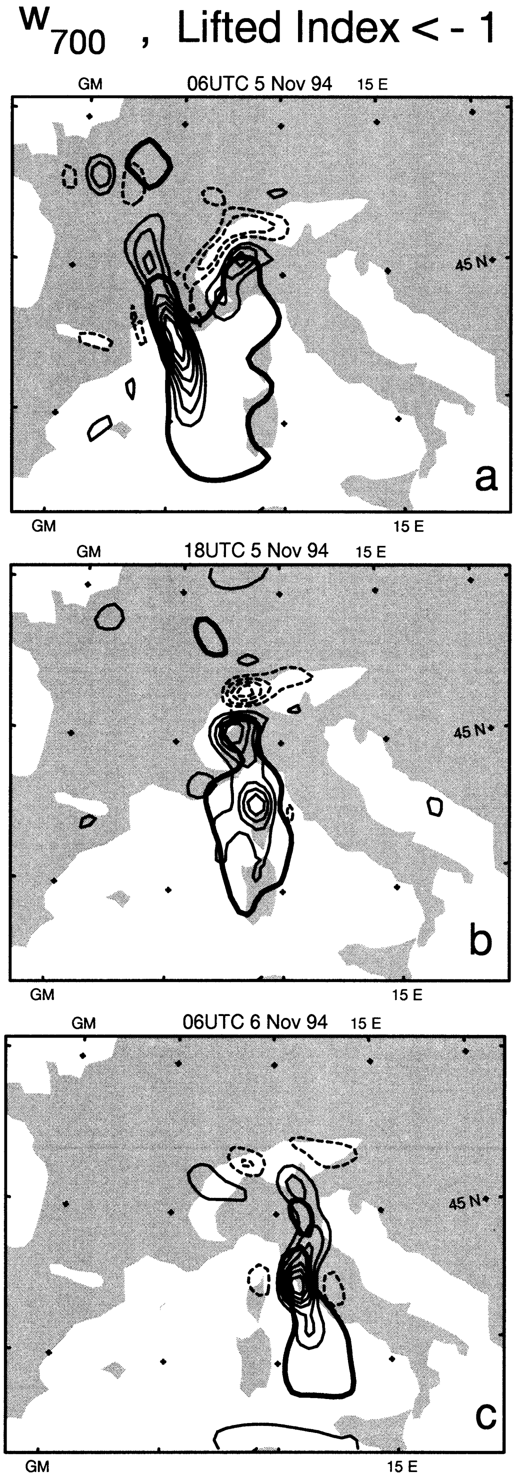

Fig. 11. 700 hPa vertical velocity w_{700} (c.i. = 5 cm s^{-1} for the first time, but thereafter c.i. = 10 cm s^{-1}; zero line is omitted and dashed lines indicate negative values here and in the remaining figures), and regions where the lifted index is less than -1 K (outlined by heavy solid line).

described by Emanuel (1985) where the adjustment to geostrophic forcing of rising motion was studied using a moist version of the Sawyer-Eliassen equation. Emanuel (1985) found that when the effectively weaker static stability of rising saturated air is accounted for, more intense rising motion is required to re-establish thermal-wind balance (in response to geostrophic forcing); by mass continuity, the stronger rising motion is over a narrower region than that of the weaker compensating subsidence occurring in the unsaturated surrounding air. Emanuel et al. (1987) applied the same approach in studying the effect of latent-heat release on the two-dimensional Eady wave, and found enhanced surface frontogenesis and southerly winds in the warm sector associated with the relatively narrow plume of rising motion (see their Fig. 7). In a similar vein, and perhaps more applicable to the present situation, Parker and Thorpe (1995), examined the effects of moist static instability in the rising air, and found an enhanced horizontal temperature gradient and a jet at low-levels in association with the intense rising motion.

Figure 13 displays a vertical cross-section through the location where there is a line of intense updraft at 1800 UTC 5 November 1994 (indicated in Fig. 12c). At 0000 UTC 5 November 1994, before there is any appreciable latent heating, Fig. 13a depicts the upper-level wave through the north-south wind component v, the characteristic upward- and westward-tilted distribution of potential temperature θ, and potential vorticity (PV) distribution. Figure 13b shows that east of the upper-level trough, the air is humid, but not saturated, and that the motion is generally upward as expected from elementary arguments (Bluestein 1993, ch. 5). At 1800 UTC 5 November 1994, Fig. 13c indicates a strong enhancement of the frontal temperature contrast and southerly wind in the lower troposphere; this enhancement is obviously associated with the narrow intense upward motion occurring in saturated air, as indicated in Fig. 13d. The evolution shown in

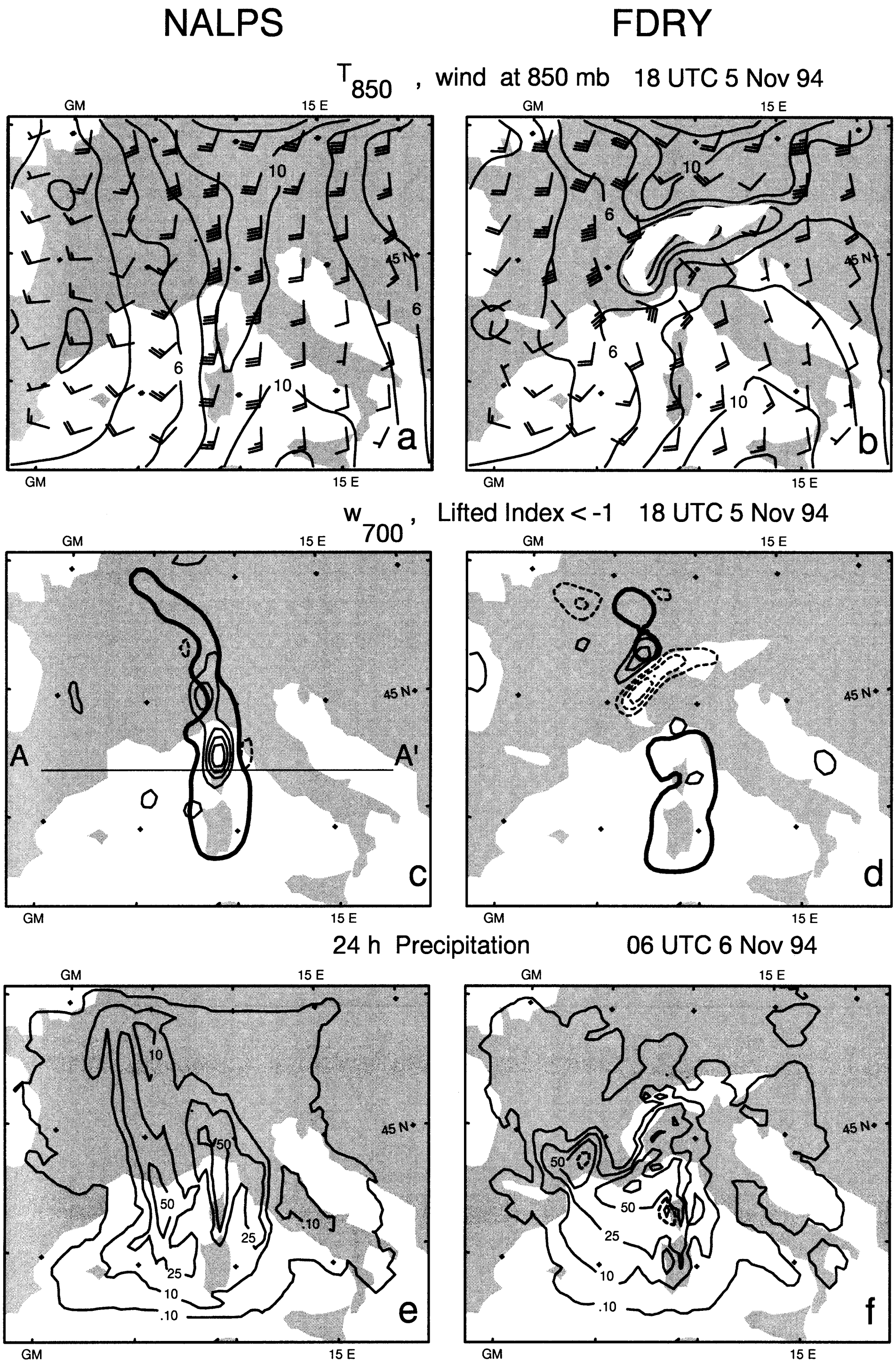

Fig. 12. Maps of the NALPS and FDRY near the time of maximum rainfall in CTRL (1800 UTC 5 November 1994). Plotting conventions in (a) and (b) as in Fig. 10d, (c) and (d) as in Fig. 11d, and (e) and (f) as in Fig. 8a.

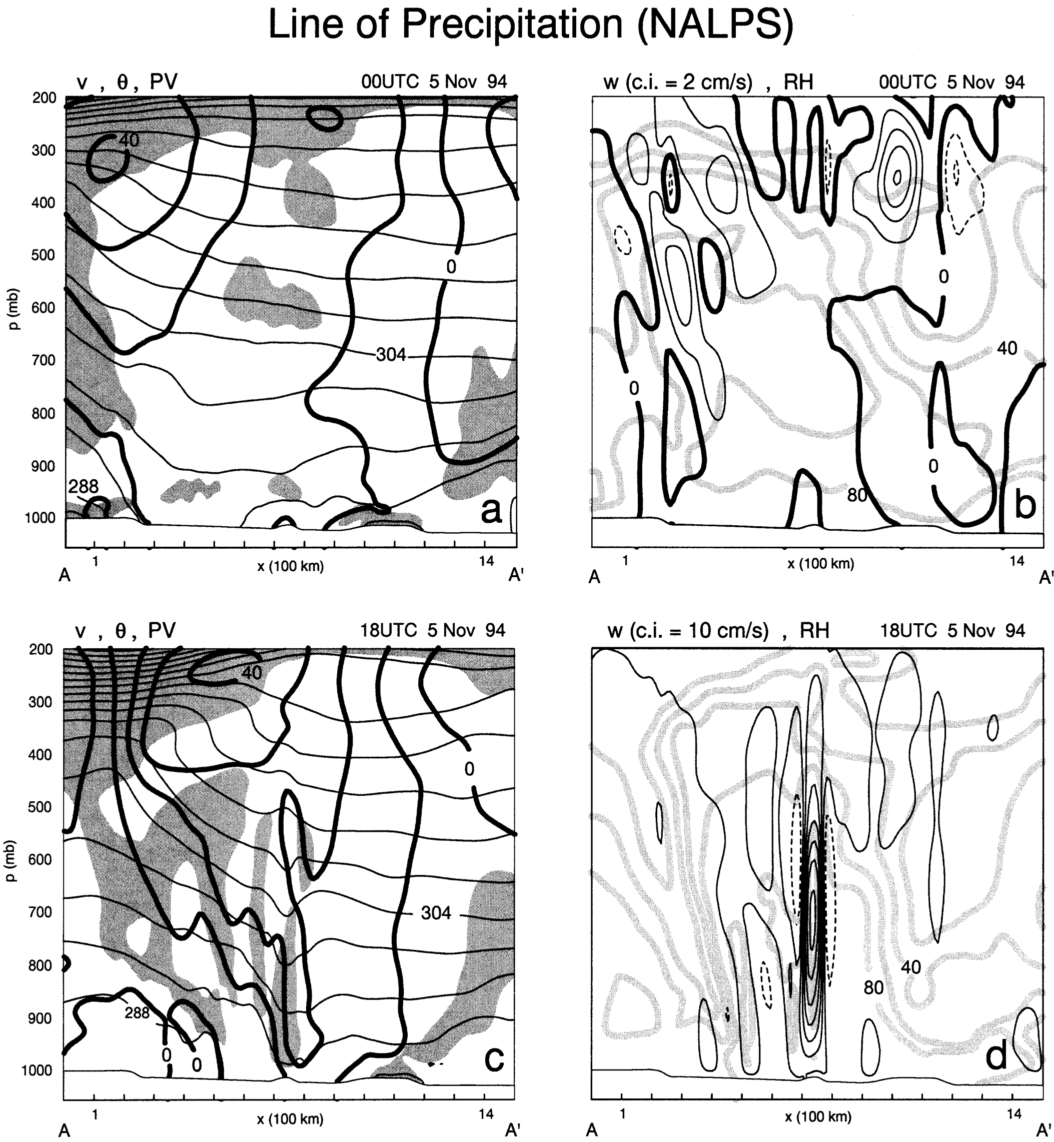

Fig. 13. Vertical cross-sections, AA′ through of the line of intense precipitation (indicated in Fig. 12c) as it occurs in the NALPS simulation showing the meridional wind v (thick solid lines c.i. = 10 m s^{-1}) and potential temperature θ (thin solid lines c.i. = 4 K), with the shaded region enclosing values of potential vorticity (PV) greater than 0.5 PVU (10^{-6} m^2 s^{-1} K kg^{-1}) at (a) 0000 UTC 5 November 1994 and (c) 1800 UTC 5 November 1994, and the vertical velocity and relative humidity RH (thick gray lines c.i. = 20%) at (b) 0000 UTC 5 November 1994 (thin solid lines c.i. = 2 cm s^{-1}, and zero line as thick solid line) and (d) 1800 UTC 5 November 1994 (c.i. = 10 cm s^{-1}, and no zero line).

Fig. 13 has the hallmarks of the "convective frontogenesis" described by Parker and Thorpe (1985). Of particular importance in the present context is the enhancement of the low-level southerlies which impinge on the southern Alps.

Latent-heat release is also an important factor in the topographic response of the flow shown in Figs. 10, 11. Fig. 12b (FDRY) shows that without latent-heat release, the southerly flow associated with the approaching front completely avoids

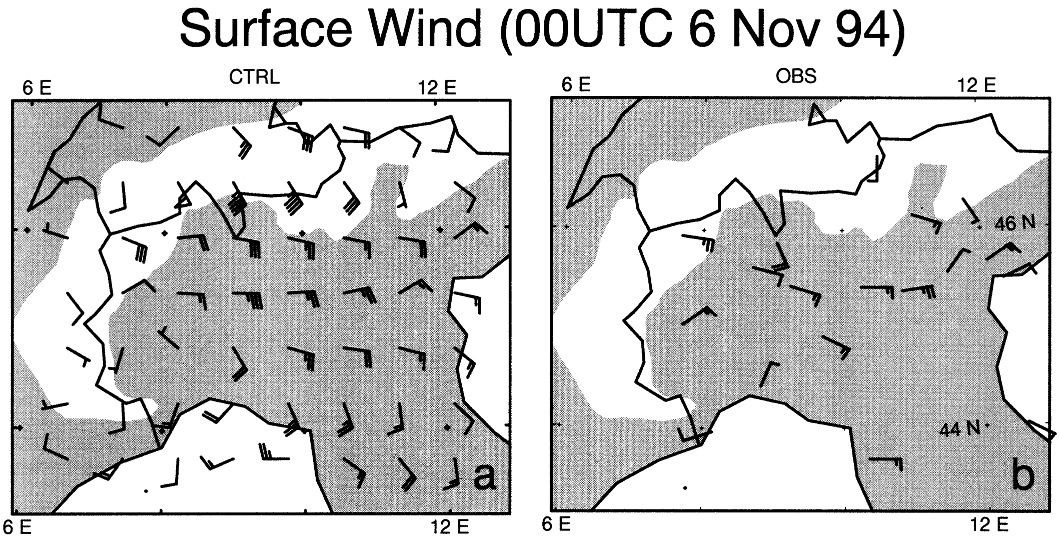

Fig. 14. Comparison of (a) model-predicted and (b) observed surface winds (one barb = 10 knots) in the nested domain (Fig. 1).

elevated terrain (including the coastal mountains) and is diverted to the west side of the Alps with little rising motion (Fig. 12d), and thereafter flows strongly through France. To a first approximation, the magnitude of the easterly flow perturbation u'/V is inversely proportional to the Froude number $\mathrm{Fr} = V/NH$, where V is the wind speed, H is the mountain height, and N is the Brunt-Väisälä frequency, a measure of the static stability. The effective static stability of the moist, southerly air stream impinging on the Alps is small, hence the flow in CTRL surmounts the Alps with slight deflection, and there is a significant orographic enhancement to the rainfall in the western Alps. Further evidence for this effect can be seen in that the maximum accumulated rainfall in FDRY (Fig. 12f) occurs away from the Alps. These experiments support the findings of Buzzi et al. (1998).

The CTRL simulation also suggests more subtle aspects of topographic enhancement of rainfall owning to the particular shape of the Alpine massif: From 1200 UTC 5 November through 0000 UTC 6 November 1994, Fig. 10 shows that the axis of maximum southerly wind progresses eastward toward the central Alps, and that the associated easterly flow deflections over the Po Valley gain in strength; strong vertical motion (Fig. 11) over the western Alps appear to be associated with these easterly wind perturbations. Moreover, these easterly wind perturbations seem to retard the motion of the precipitation system over the western Alps. Fig. 14 shows the lowest model sigma level (40 m AGL) winds for the CTRL (Fig. 14a) and a network of observed surface (10 m) winds (Fig. 14b) at 0600 UTC 6 November 1994; the observations support the model prediction of easterly wind in the Po Valley, and a small-scale cyclonic wind perturbation near the tip of the southern Alps.

The foregoing description bears a fair resemblance to the mechanism investigated by Orlanski and Gross (1994; see their Figs. 15, 16) for the retardation of a eastward-moving front on the south side of an Alps-like obstacle, and the subsequence small-scale cyclogenesis on the south side (the analogous Gulf of Genoa). In the FDRY case shown in Fig. 12, evidence of the mechanism described by Orlanski and Gross (1994) is seen in that the front is retarded on the south side of the Alps, and there is the beginnings of a cyclonic circulation over the Mediterranean. As remarked upon by these authors, significant modifications to their theory, which is based on dry dynamics, could be expected with the inclusion of latent-heat release. In CTRL (Fig. 10), there is a cyclonic circulation south of the Alps, but rather than being located in the Gulf of Genoa, it is located over northwestern Italy. Figs. 15a–b show

700 hPa-level vorticity in CTRL at 1800 UTC 5 November 1994 and 0000 UTC 6 November 1994 respectively; there is a line of strongly positive relative vorticity which slowly moves eastward and grows in strength. Comparison of Figs. 15a, b with the relevant times of Fig. 11 indicates a strong connection between latent-heat release, upward motion aloft and positive vorticity production. In FDRY (Fig. 15c), on the other hand, the vorticity is mainly negative over the Alps, as expected from elementary arguments (Smith, 1979).

Although more research is required for definitive answers, several observations can be made at this point concerning the role of latent-heat release on topographic flow effects occurring in connection with the Piedmont flood. The first is that latent-heat release is essential in describing even the qualitative flows features [mountain anticyclone (dry) vs. mountain cyclone (wet)] over the Alps. More speculatively, our impression from CTRL is that the sideways-"L" shape of the western Alps is a likely contributor of the slow movement of precipitation system there. Unstable air lifted by the western Alps (the short leg of the sideways "L") may produce positive vorticity through latent-heat-induced vortex stretching. This vorticity modifies subsequent development by inducing easterly wind perturbations towards the concave part of the sideways L (i.e. Piedmont) which both retard the eastward progress of the precipitation system, and induce further lifting of unstable air, latent-heating and vorticity production over the western Alps, all of which are conducive to flooding. When the cold front ultimately passes to the east of the western Alps (Fig. 10, 0600 UTC 6 November 1994), the moist air in the Po Valley begins to be replaced by the stable post-frontal air, and rainfall diminishes. Hence the spatially inhomogeneous distribution of the moist static stability is also an important factor in understanding the topographic-flow effect.

6. Summary

In the present study, we have examined the meteorological conditions attending the Piedmont

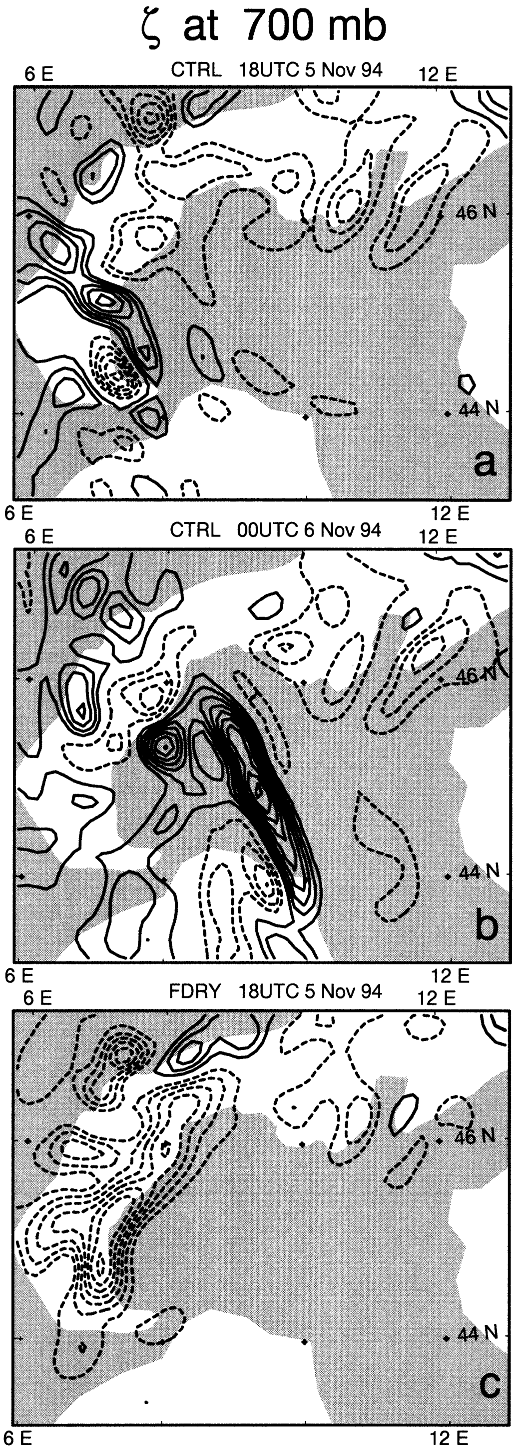

Fig. 15. Vertical vorticity (c.i. $= 1 \times 10^{-4}$ s^{-1}) at 700 hPa from CTRL (upper 2 panels) and (c) FDRY in the nested domain (Fig. 1).

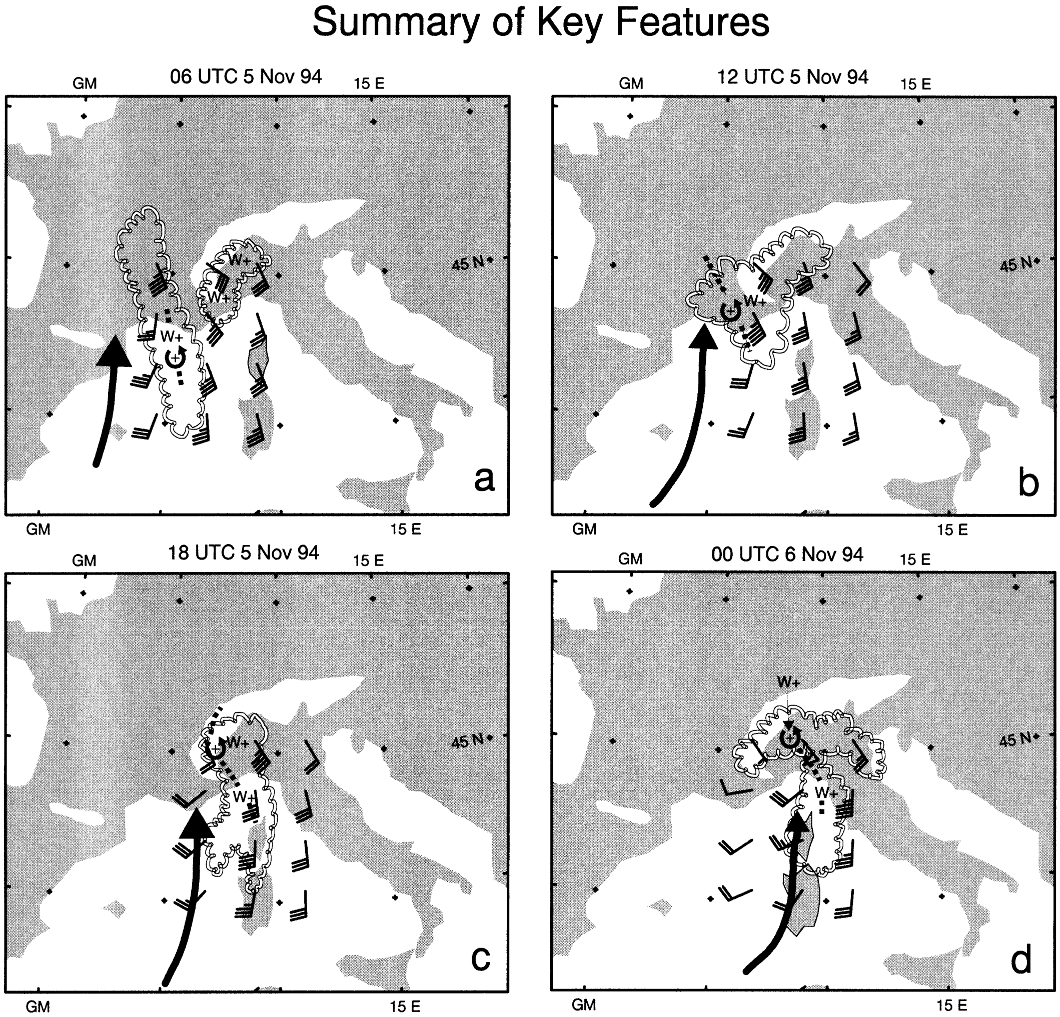

Fig. 16. Summary of the key meteorological components leading to the Piedmont flood. The thick arrow indicate the jet axis at 500 hPa. Wind barbs are a subset of 850 hPa winds shown in Fig. 10. Curly lines indicate rising motion greater than 10 cm s^{-1}, and W_+ indicates the position of the updraft maximum. Position of positive vorticity maximum indicated by curled arrow, and axis of vorticity maximum is indicated by the dashed line.

flood of 5 November 1994 using the newly implemented the Emanuel (1991, 1993) cumulus-parameterization scheme in the MM5 modeling system. Overall agreement between the model-predicted precipitation fields in and around the flood region is good. The present simulations indicate the dominance of explicit processes in the flood region and produced simulations consistent with two recent modeling studies of the Piedmont flood (Buzzi et al., 1998; Romero et al., 1998).

Sensitivity tests helped in the identification of the key physical factors leading to the Piedmont flood. Fig. 16 contains a schematic diagram that summarizes our findings. At 0600 UTC 5 November 1994 (Fig. 16a), a precursor mobile upper-level trough is depicted; associated synoptic-scale rising motion is enhanced as it encounters the conditionally unstable air over the Mediterranean. The intensified rising motion takes the form of a convective line that is associated with a strong low-level horizontal temperature gradient and southerly flow. As the line approaches the western edge of the Alps (Fig. 16b), rising motion is enhanced by orographic lifting of conditionally unstable air; positive vorticity is produced through vortex stretching. We believe this vorticity induces the easterly flow perturbation that is instrumental in retarding the eastward movement of the line over the Piedmont region (Figs. 16c, d), and possibly enhances orographic precipitation over the upper part of the Po Valley.

Another possible contributor to convergent motion over Piedmont region that needs further exploration is the effect of horizontal variation of the moist static stability in the air stream impinging on the Alps. In the present case, the moist southerly air impinging on the Alps becomes progressively drier with distance eastward. Hence it is possible that on the west side, the high values of the Froude number in the moist air stream allow the flow to go over the Alps while the stronger stability of air to the east produces stronger easterly flow perturbations and thus a convergence of the flow in the flood area. Further study involving more complex representations (e.g., "L" shapes) of Alpine topography, combined with the effects of latent-heat heat release, is needed.

7. Acknowledgements

The Mesoscale Alpine Programme (MAP) is acknowledged for the ECMWF analysis and precipitation data (Map data center). This research was partially supported by NCAR during a visit and by Italian National Research Council (CNR). Comments on the first draft of this paper by J. Bresch, G. Hakim, and C. Davis are gratefully acknowledged.

REFERENCES

Benjamin, S. G. 1983. *Some effects of surface heating and topography on the regional severe storm environment*. PhD thesis, Department of Meteorology. The Pennsylvania State University, 265 pp.

Binder, P. et al. 1996. *MAP — Mesoscale Alpine Programme design proposal.* MAP Programme Office, 77pp. (Available from MAP Programme Office c/o Swiss Meteorological Institute, Krahbuhlstrasse 58, CH-8044 Zurich, Switzerland.)

Bluestein, H. B. 1993. *Synoptic-dynamics meteorology in midlatitudes*, vol. I. Oxford University Press, 431 pp.

Boni, G., Conti, M., Dietrich, S., Lanza, L., Marzano, F. S., Mugnai, A., Panegrossi, G. and Siccardi, F. 1996. Multisensor observations during the flood event of 4–6 November, 1994 over Northern Italy. *Remote Sensing Reviews* **14**, 91–117.

Buzzi, A., Tartaglione, N. and Malguzzi, P. 1998. Numerical simulations of the 1994 Piedmont flood: Role of orography and moist processes. *Mon. Wea. Rev.* **126**, 2369–2383.

Doswell, C. A., Ramis, C., Romero, R. and Alonso, S. 1998. A diagnostic study of three heavy precipitation episodes in the western Mediterranean region. *Wea. and Forecasting*. **13**, 102–124.

Dudhia, J. 1989. Numerical study of convection observed during the winter monsoon experiment using a mesoscale two-dimensional model. *J. Atmos. Sci.* **46**, 3077–3107.

Dudhia, J. 1993. A nonhydrostatic version of the Penn State-NCAR mesoscale model: Validation tests and simulation of an Atlantic cyclone and cold front. *Mon. Wea. Rev.* **121**, 1493–1513.

Emanuel, K. A. 1985. Frontal circulation in the presence of small moist symmetric stability. *J. Atmos. Sci.* **42**, 1062–1071.

Emanuel, K. A., Fantini, M. and Thorpe, A. J. 1987. Baroclinic instability in an environment of small stability to slantwise moist convection. *J. Atmos. Sci.* **44**, 1559–1573.

Emanuel, K. A. 1991. A scheme for representing cumulus convection in large scale models. *J. Atmos. Sci.* **21**, 2313–2335.

Emanuel, K. A. 1993. A cumulus representation based on the episodic mixing model: The importance of mixing and microphysics in predicting humidity. The Representation of cumulus convection in numerical models. *Meteor. Monogr.* **46**, Amer. Meteor. Soc., 185–192.

Emanuel, K. A. 1994. *Atmospheric convection.* Oxford University Press, 580 pp.

Massacand, A. C., Wernli, H. and Davies, H. C. 1998. Heavy precipitation on the Alpine southside: An upper-level precursor. *Geophys. Res. Lett.* **25**, 1435–1438.

Orlanski, I. and Gross, B. D. 1994. Orographic modification of cyclone development. *J. Atmos. Sci.* **51**, 589–611.

Parker, D. J. and Thorpe, A. J. 1995. Conditional convective heating in a baroclinic atmosphere: a model of convective frontogenesis. *J. Atmos. Sci.* **52**, 1699–1711.

Romero, R., Ramis, C., Alonso, S., Doswell, C. A. and Stensrud, D. J. 1998. Mesoscale model simulations of three heavy precipitation events in the western Mediterranean region. *Mon. Wea. Rev.* **126**, 1859–1881.

Senesi, S., Bougeault, P., Cheze, J. L., Cosentino, P. and Thepenier, R. 1996. The Vaison-la Romaine flash

flood: Meso-Scale analysis and predictability issues. *Wea. Forecasting* **11**, 417–442.
Smith, R. B. 1979. The influence of mountains on the atmosphere. *Advances in Geophysics* **21**.
Zhang, D.-L. and Anthes, R. A. 1982. A high-resolution model of the planetary boundary layer: sensitivity tests and comparisons with SESAME-79 data. *J. Appl. Met*. **21**, 1594–1609.